Ablation by ultrashort laser pulses: Atomistic and thermodynamic analysis of the processes at the ablation threshold

Arun K. Upadhyay,[1] Nail A. Inogamov,[2] Bärbel Rethfeld,[3] and Herbert M. Urbassek[3,*]
[1]*Department of Materials Science and Engineering, University of Michigan, Ann Arbor, Michigan 48109-2136, USA*
[2]*Landau Institute for Theoretical Physics, Russian Academy of Science, Kosygina 2, 117940 Moscow, Russia*
[3]*Fachbereich Physik, Universität Kaiserslautern, Erwin-Schrödinger-Straße, D-67663 Kaiserslautern, Germany*
(Received 1 February 2008; revised manuscript received 12 May 2008; published 31 July 2008)

Ultrafast laser irradiation of solids may ablate material off the surface. We study this process for thin films using molecular-dynamics simulation and thermodynamic analysis. Both metals and Lennard-Jones (LJ) materials are studied. We find that despite the large difference in thermodynamical properties between these two classes of materials—e.g., for aluminum versus LJ the ratio $T_c/T_{\rm tr}$ of critical to triple-point temperature differs by more than a factor of 4—the values of the ablation threshold energy $E_{\rm abl}$ normalized to the cohesion energy, $\epsilon_{\rm abl}=E_{\rm abl}/E_{\rm coh}$, are surprisingly universal: all are near 0.3 with $\pm 30\%$ scattering. The difference in the ratio $T_c/T_{\rm tr}$ means that for metals the melting threshold ϵ_m is low, $\epsilon_m<\epsilon_{\rm abl}$, while for LJ it is high, $\epsilon_m>\epsilon_{\rm abl}$. This thermodynamical consideration gives a simple explanation for the difference between metals and LJ. It explains why despite the universality in $\epsilon_{\rm abl}$, metals thermomechanically ablate always from the liquid state. This is opposite to LJ materials, which (near threshold) ablate from the solid state. Furthermore, we find that immediately below the ablation threshold, the formation of large voids (cavitation) in the irradiated material leads to a strong temporary expansion on a very slow time scale. This feature is easily distinguished from the acoustic oscillations governing the material response at smaller intensities, on the one hand, and the ablation occurring at larger intensities, on the other hand. This finding allows us to explain the puzzle of huge surface excursions found in experiments at near-threshold laser irradiation.

DOI: 10.1103/PhysRevB.78.045437 PACS number(s): 79.20.Ds, 79.20.Ap, 61.80.Ba, 02.70.Ns

I. INTRODUCTION

In this work we present molecular-dynamics simulations of the expansion of condensed matter energized on a very short time scale. This corresponds to the case of absorption of an ultrashort laser pulse, where the excitation time is short in comparison with the time of stress relaxation. Previous studies[1–7] have shown the following mechanism to be responsible for the ablation of solids under ultrafast laser irradiation. The high-energy density delivered to the solid by the laser leads to an initially nearly isochoric heating of the material. The time scale for expansion is much larger than the laser-pulse duration. The resulting huge compressive thermoelastic pressure lets the material expand. A rarefaction wave starts from the surface of the material and propagates inward. Unloading of the stress causes the appearance of tensile stresses. The ensuing material processes depend on the energization strength.

For sufficient energization strength, an important consequence of the tensile pressure will be the macroscopic *ablation* of the target; this term is used in contrast to sublimation or evaporation processes induced by the laser heating of the solid, which occur at smaller laser intensities. We note that evaporation also takes place at higher intensities, but above the ablation threshold the amount of the evaporated material is small in comparison with the amount of the thermomechanically ablated material. The ablation process is basically described as the tearing (or rupture or fragmentation) of the material. We note that it has also been described as *spallation*, even though this name is restricted to processes occurring in the solid state, or to be initiated by *cavitation*—a term describing the formation of gas bubbles in a liquid under tensile stress. Ablation of metals has been shown to be initiated by the nucleation of voids in the material, which grow under the tensile pressure until the material fragments.[4,8,9] In these studies, the laser-irradiated material was already molten before the void nucleated. As will be shown in this study, Lennard-Jones materials behave differently, in that near-threshold ablation occurs in the solid rather than the liquid state.

At higher laser intensities, the spallation plate becomes increasingly thinner and disappears at the called fragmentation[10] or evaporation threshold.[11] Finally, at even higher laser intensities, the irradiated material fragments to a vapor plume, consisting of clusters (droplets) with a wide size distribution.[10] This process is sometimes called explosive (or volume) evaporation or *phase explosion*.[12] This latter term emphasizes the fact that the irradiated material has moved deep into the metastable region of the phase diagram and approaches the spinodal line; here fluctuations in density, temperature, and pressure grow, leading to a rapid phase transition of the material to a two-phase mixture. The processes occurring below the ablation threshold, on the other hand, have been investigated primarily with respect to the melting process induced.[5]

In the present paper, we wish to concentrate on the processes occurring at laser intensities in the vicinity of the ablation threshold. Using molecular-dynamics simulations, we study the fragmentation of solids, the nucleation and temporal evolution of voids, and the thermodynamic pathways of the material through different phases. Our results will be compared with the macroscopic thermodynamic analysis of the material behavior. Two different classes of materials will be investigated, metals—where cohesion is provided by the

delocalized metallic binding, which is modeled by many-body potentials—and the so-called "Lennard-Jones" material, which is prototypical of matter held together by localized bonds, modeled by pair potentials. As the phase diagrams of these two classes of materials are quantitatively different, we shall investigate the resulting similarities or differences in the material behavior.

II. SYSTEM

We study the expansion of a laser-irradiated freestanding film. For simplification, it is assumed that the laser irradiation energizes the film homogeneously. As a further simplification, we model the laser irradiation to be instantaneous, i.e., the laser energy is given to the atoms immediately at the start of the simulation. While in the simulation of any real experiment, the finite laser-pulse width and the electron-phonon relaxation time will delay and smoothen the energy transfer from the electronic to the atomic system, in this investigation we will not consider this effect. The influence of the electronic material properties would be conveniently performed in terms of the two-temperature model[13] and has been reported elsewhere.[4,5,7,14,15]

We perform simulations both on a Lennard-Jones material and for various metals. Most results will be shown for the special case of an Al target, but also the materials Cu, Ti, and W have been investigated.[16] The interatomic potentials employed in the simulation of these metals are the many-body potentials of Ref. 17 for Cu, Ref. 18 for Al, and Ref. 19 for Ti and W. We note that these potentials have been designed such as to correctly reproduce the ground-state crystal structure, the cohesive energy E_{coh} (Al: 3.39 eV, Cu: 3.49 eV, Ti: 4.85 eV, and W: 8.90 eV), and the bulk modulus B of these materials.

A Lennard-Jones material is characterized by two material parameters only, the Lennard-Jones energy scale ϵ_{LJ} and the length parameter σ. Thus, frequently, data are presented in scaled units, i.e., density is normalized to σ^{-3}, temperature to ϵ_{LJ}/k, where k is Boltzmann's constant, and pressure to $\epsilon_{\mathrm{LJ}}/\sigma^3$. We note that the cohesive energy of a Lennard-Jones material is $E_{\mathrm{coh}}=8.6\epsilon_{\mathrm{LJ}}$.

In our simulations, the films have a thickness of typically 20–30 monolayers (ML) and a lateral cross section of between 20×20 and 36×36 ML. Laterally, periodic boundary conditions are employed, while the top and bottom surfaces are free. For the fcc crystallite, the top and bottom surfaces have a (100) crystallography, and the total number of atoms in our simulation cell amounts to 4000 atoms. For the hcp crystallite, the surfaces have a (0001), and for the bcc structure, a (100), crystallography; in these cases 2000 atoms were simulated. At time $t=0$, the film is energized by giving each atom a kinetic energy E_0. In the simulation this is accomplished by assigning each atom a velocity $\sqrt{2E_0/M}$ in random direction, where M is the atom mass. The simulations have been followed until up to 30–100 ps after irradiation. This time is long compared to the typical time scale of the material, the *acoustic time*,

$$t_{\mathrm{sound}} = L/v_{\mathrm{sound}}, \tag{1}$$

which a sound wave of velocity v_{sound} needs to pass through the film of thickness L. For our systems, t_{sound} is of the order of 1 ps.

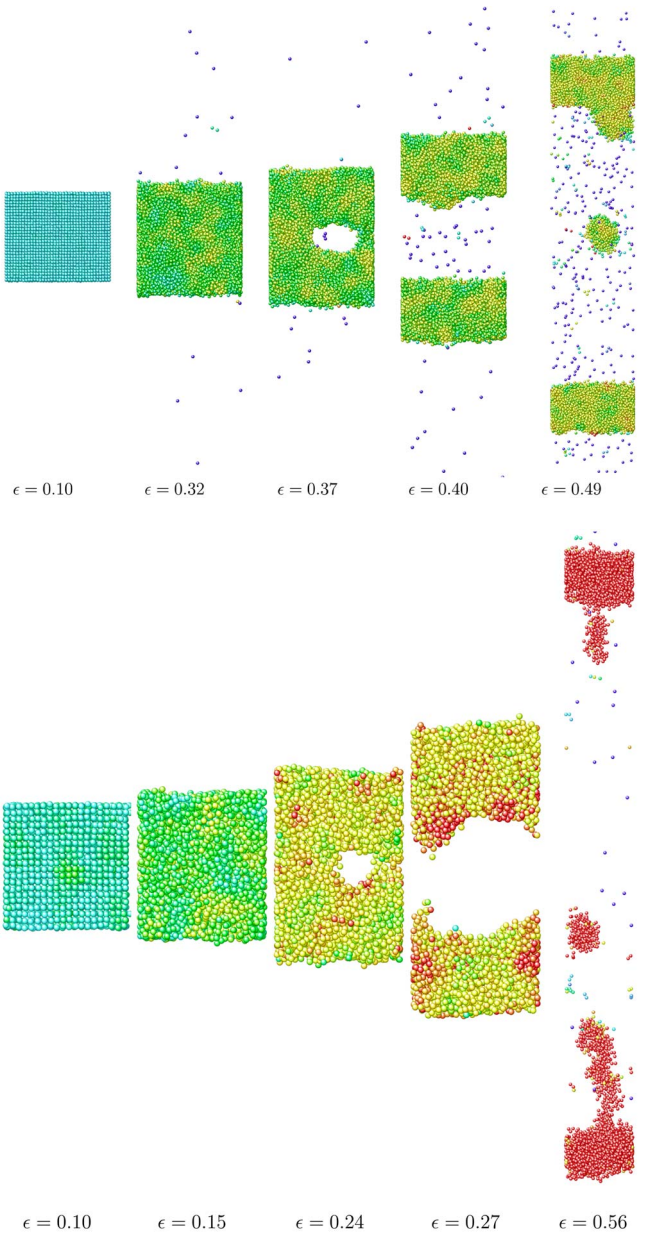

FIG. 1. (Color online) Series of snap shots of (a) the energized Lennard-Jones film and (b) the Al film (Ref. 16), featuring the materials processes investigated. The energization ϵ [Eq. (3)] is indicated in the figures. Data have been taken at a time $t \gg t_{\mathrm{sound}}$, typically between 5 and 20 ps after energization. Color denotes the local temperature and increases from blue to red; green characterizes the melting point. The subplots visualize from left to right the effect of increasing energization: crystalline solid; molten; temporary void formation; spallation, cluster formation.

In the following, we shall call the energy E_0 imparted at time $t=0$ to each atom the energy transfer or "energization." In the simulation, this energization process is realized by giving each atom at time $t=0$ a kinetic energy E_0, with random direction of the velocity.[20] We performed test simulations to verify that the dynamics of void nucleation is independent of the initial velocity distribution (for identical energization E_0). The reason hereto is that a Maxwellian dis-

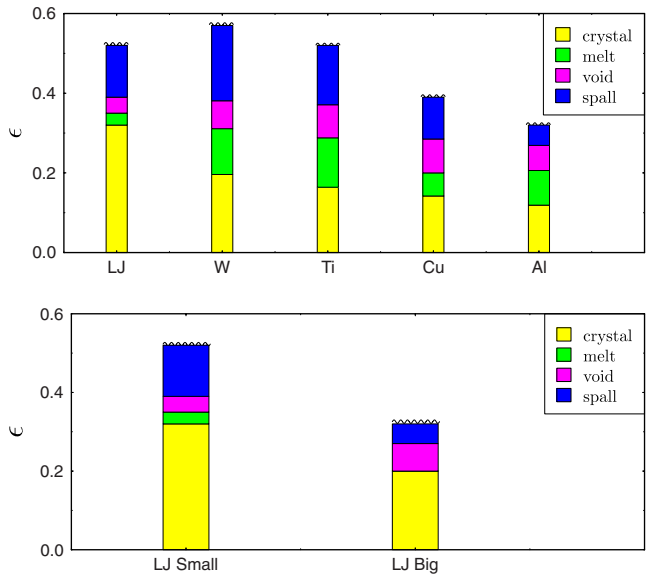

FIG. 2. (Color online) Synopsis of energization thresholds, $\epsilon = E_0/E_{\mathrm{coh}}$, (a) for the Lennard-Jones film and for four metals (Ref. 16) and (b) for a "small" and a big Lennard-Jones film (see text).

tribution is established within less than 1 ps, while voids need several 10 ps to start nucleating.

In our model, the energization E_0 is the sole characteristics of the laser irradiation which enters the model. It is connected to the *absorbed* laser fluence Φ via the thin-film width L and the atomic number density n through

$$\Phi = E_0 L n. \tag{2}$$

In order to compare data for the different materials studied, we shall normalize the energy E_0 to the cohesive energy E_{coh} of the material,

$$\epsilon = \frac{E_0}{E_{\mathrm{coh}}}. \tag{3}$$

We determine temperature and pressure in our simulation as local quantities, which are averaged over around 50 atoms to reduce fluctuations.[21] These local quantities can be used to generate atomistic plots and animations of the irradiated solid (cf. Figs. 1 and 4). Since these quantities are not uniform in the film,[4,5,20] we also record spatially averaged quantities. In these, we usually average over the *central third* part of the system, i.e., over all atoms whose distance from the center of the irradiated slab is less than a third of the distance of the outermost atoms.

III. RESULTS

A. Universality of material response

In Fig. 1 the response of a thin film of material energized homogeneously with various values of energy E_0, corresponding to different strengths of the initial excitation, is presented. These data have been taken at a time, which is large compared to the acoustic time t_{sound}. With increasing E_0, the material is liquefied, voids appear, until the material

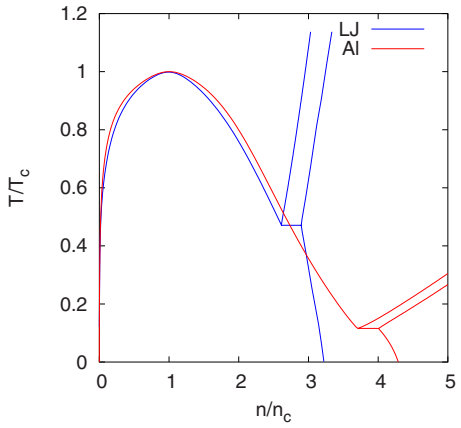

FIG. 3. (Color online) Normalized phase diagram of a Lennard-Jones material and of Al as a typical metal. Temperature T and density n have been normalized to their values at the critical point, T_c and n_c.

breaks (ablation), and finally a regime of multifragmentation and cluster formation appears. A comparison of Fig. 1(a) for a Lennard-Jones material and Fig. 1(b) for Al shows that these mechanisms occur universally and independently of the target material. However, details differ: thus evaporation is stronger for the Lennard-Jones material than for the metal; on the other hand, the cluster sizes in the multifragmentation stage show a more varied distribution than the clusters formed in a metallic target.

In Fig. 2(a) we compare the energization thresholds above which the materials response is characterized by melting,

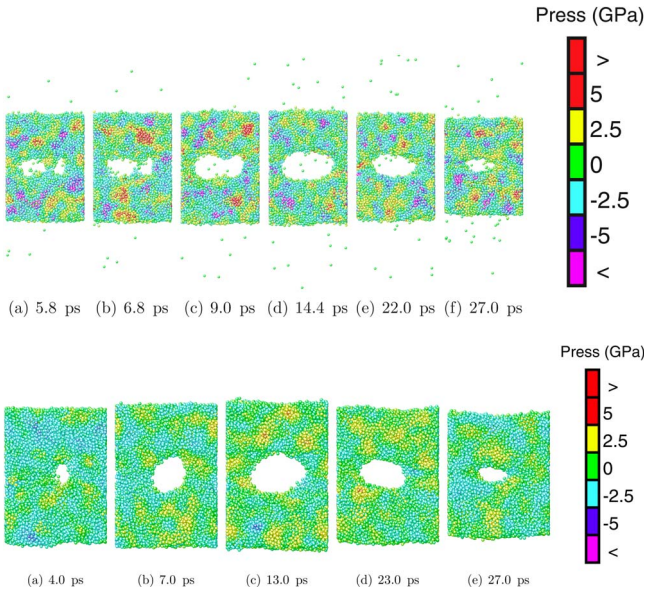

FIG. 4. (Color online) Series of snap shots showing void growth and decay (a) in a Lennard-Jones film and (b) in a Cu film. A cross section through the film is shown, which has free top and bottom surfaces, while laterally periodic boundary conditions are used. The slab is energized homogeneously at time $t=0$ to $E_0=0.8$ eV/atom, corresponding to $\epsilon=0.23$ for the Cu metal and to $E_0=1.33$ eV/atom, corresponding to $\epsilon=0.37$ for the Lennard-Jones material. Atoms are colored according to their local pressure. Positive pressures are compressive; negative pressures are tensile.

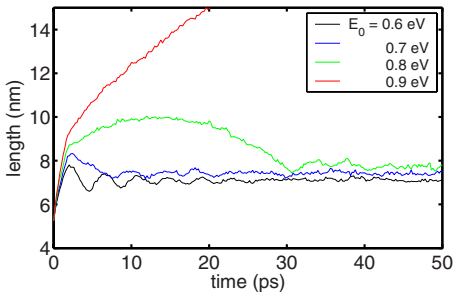

FIG. 5. (Color online) Time evolution of the thickness of a Cu film after energization E_0 around the ablation threshold.

void formation, or ablation. The data for the four metals treated (W, Ti, Cu, and Al) have been taken from Ref. 16. The thresholds are normalized to the cohesive energy E_{coh} of the material, $\epsilon = E_0/E_{\mathrm{coh}}$ [Eq. (3)]. We see that the actual threshold energies vary between the materials. In particular, the Lennard-Jones material differs from the metals studied in that (i) its melting threshold is higher than for all the metals considered and (ii) the window of energizations, where melting—and also spallation—occurs is smaller than for the metals.

In order to understand the origin of this different behavior, we plot in Fig. 3 the phase diagrams of a Lennard-Jones material and that of Al, as a typical metal. The Lennard-Jones data have been taken from Refs. 22–26, while the Al data are due to Ref. 27. By normalizing temperature and density to their values at the critical point, the main difference between a Lennard-Jones material and a metal becomes evident: the metal has a relatively small triple-point temperature and hence a broad range of temperatures and densities, where a liquid phase exists. We may discuss the width of the liquid region with the help of the ratio of critical to triple-point temperature. These ratios are 2.1 for the Lennard-Jones material and 9.0 for Al. Thus the widths of the liquid zone differ by a factor of 4.2 (on a temperature scale).

These characteristics of the phase diagrams are connected with the material response summarized in Fig. 2(a). The threshold for melting is higher for the Lennard-Jones material than in all the metals considered; on the other hand, the range of energies leading to melting is very small in this material, as the Lennard-Jones phase diagram exhibits only a small melting range.

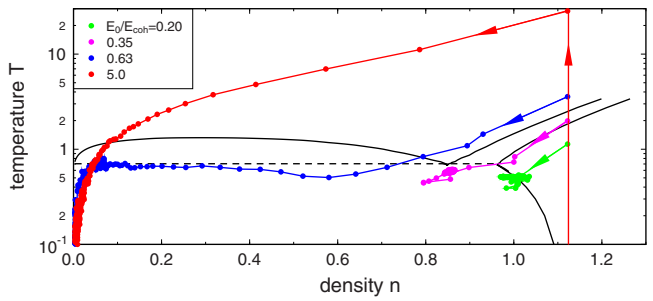

FIG. 6. (Color online) Phase-space (T-n) trajectories of the path of the simulation volume in a laser-irradiated Lennard-Jones film (Ref. 41). Data are given in Lennard-Jones units, i.e., density is normalized to σ^{-3} and temperature is normalized to ϵ_{LJ}/k. Four different energizations $\epsilon = E_0/E_{\mathrm{coh}}$ have been studied. The phase boundaries of the Lennard-Jones system (see Fig. 3) have been included (full lines). The horizontal dashed line indicates the triple-point temperature.

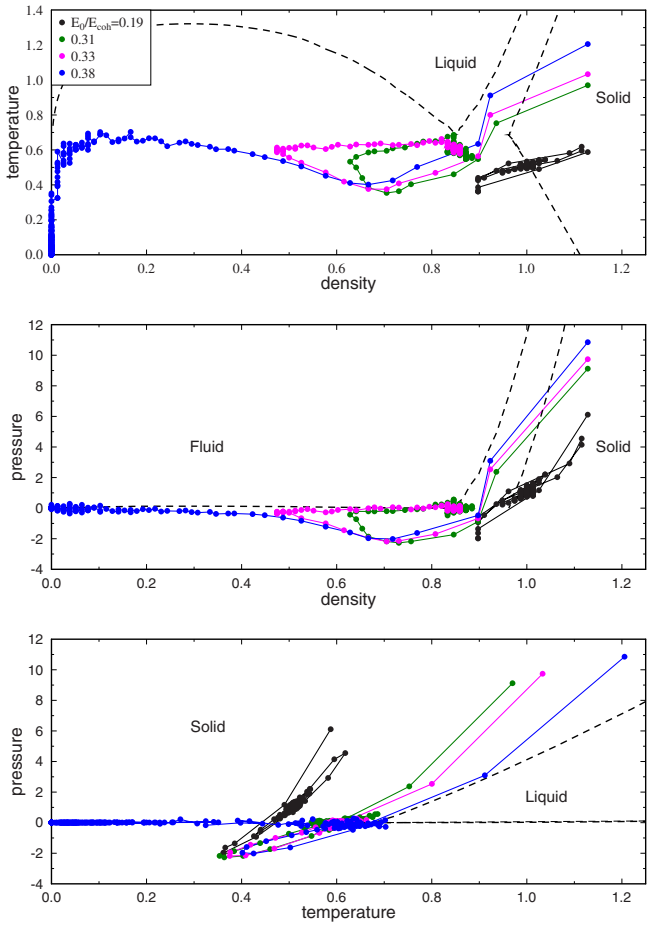

FIG. 7. (Color online) Phase-space trajectories of central third of simulation volume in a Lennard-Jones film. Data are given in Lennard-Jones units. Four different energizations have been studied. The dashed lines indicated the Lennard-Jones phase diagram; the "fluid" phase indicated in the top subfigure denotes the homogeneous phase above the critical temperature. Top: T-n trajectories. Middle: p-n trajectories. Bottom: p-T trajectories.

Anisimov and co-workers[3,7,28] performed a series of simulations on Lennard-Jones systems, in which a considerably larger simulation volume was employed. It is therefore of interest to study the influence of the size of the simulation volume on the material response zones. To this end, we performed a simulation with a "big" Lennard-Jones crystallite, in which the crystal thickness has been increased by a factor of 10 to 300 ML; this corresponds to an increase in thickness from 23σ to 230σ in Lennard-Jones units. Figure 2(b) shows a definite size effect. Ablation occurs at smaller energizations, $\epsilon = 0.26$, instead of the higher value of $\epsilon = 0.39$ for the 30 ML film. Anisimov *et al.*[28] reported a value of $\epsilon = 0.28$ for their film of thickness 1680σ, in fair agreement with our result; the deviations are due to the broader target used in that study and to the use of a truncated potential. The value found for the larger Lennard-Jones films is comparable to the value found for the most refractory metal studied, W, in Fig.

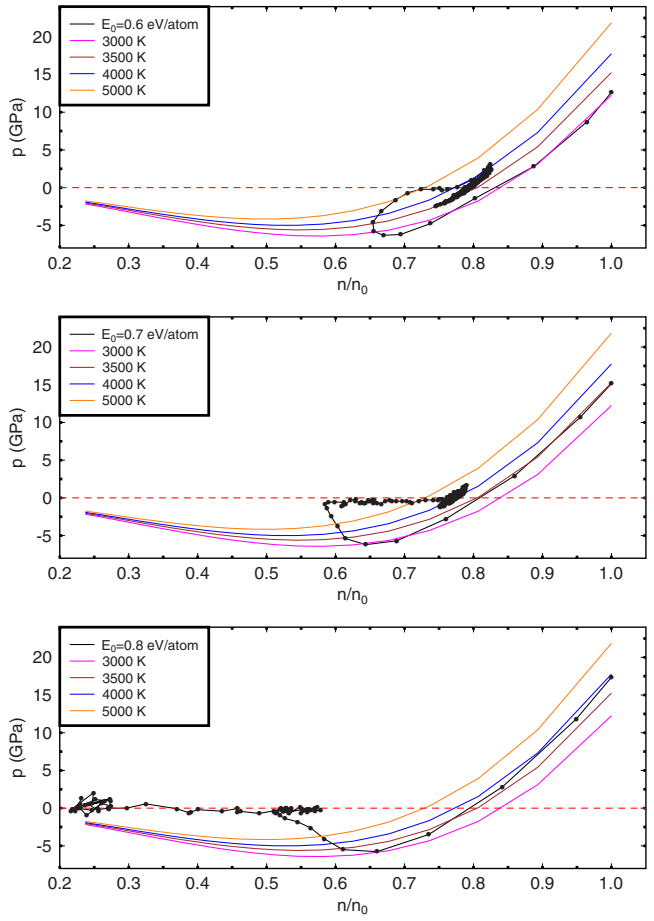

FIG. 8. (Color online) Phase-space (p-n) trajectories of the central third of the simulation volume in an Al film energized to E_0 =0.6 eV/atom (top), E_0=0.7 eV/atom (middle), and E_0=0.8 eV/atom (bottom). Density n has been normalized to the initial solid density, n_0. The molecular-dynamics trajectories (data taken every 0.2 ps) are compared to a set of isentropes calculated from a realistic equation of state for Al.

2(a). We assume that the higher resistivity of the ultrathin film to spallation reflects the strength of an undamaged crystallite toward tensile loading: For the thicker film, spallation is preceded by plastic deformation and damage buildup,[29] which weaken the crystal and make spallation possible already at energizations of ϵ=0.26, where the ultrathin film is still undamaged and has a higher strength.

A simple estimate of the effect of film thickness follows from the theory of gas bubble nucleation in liquids.[30,31] The nucleation time τ can be expressed as the product of a pre-exponential factor P and the exponential factor $\exp(W/kT)$, where T is the temperature and k is the Boltzmann constant. The work W for creating a critical nucleus can be estimated as

$$W = \frac{16\pi\sigma^3}{3p^2}, \tag{4}$$

where p is the (negative) pressure and σ is the surface tension. Both the pressure and temperature at the start of nucleation depend on the initial energization E_0, and they grow with increasing E_0, while they are unaffected by L. Hence E_0 enters the exponential factor, while the thickness L of the film only enters the pre-exponential factor P. Since the time the system stays under tensile stress is proportional to the acoustic time, $t_{\text{sound}}=L/v_{\text{sound}}$ [Eq. (1)], the material in a thick film can simply wait longer until a void nucleates—the nucleation time being essentially unaffected by the film thickness. Therefore the threshold $E_0^{\text{thr}}(L)$ decreases with increasing L, but only as a weak logarithmic function. Strictly speaking, the above estimate only applies for homogeneous conditions; however, the difference between homogeneous vs inhomogeneous conditions is not essential, as it only enters the pre-exponential factor.

Even more astonishingly, the small window of energization, where the small crystal melted without spallation, has disappeared: the material undergoes spallation in its solid rather than liquid state. The suppression of the melt zone is a simple consequence of the fact that in larger crystals, a smaller excitation is sufficient for ablation. The higher ablation threshold for the thinner film moves the threshold adiabat for the thinner film to a higher position in the n-T phase plane; thus it intersects the binodal slightly above the triple point. In contrast, for the thicker film, the threshold adiabat lies lower (below the triple point) and intersects the binodal below the triple point, and the liquid phase does not appear.

Recently,[32] the *threshold adiabats* were investigated, i.e., those adiabats along which a material energized at its ablation threshold expands. It was demonstrated that for a Lennard-Jones material, the threshold adiabat passes through the triple-point region of the phase diagram (cf. Fig. 6); as a consequence ablation may occur without melting. For a metal, however, the threshold adiabat enters the coexistence region far above the triple point. This is a direct consequence of the wide region occupied by the liquid state in the phase

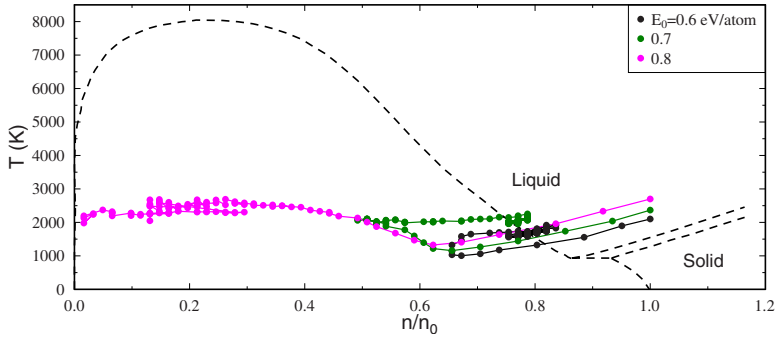

FIG. 9. (Color online) Phase-space (T-n) trajectories of the central third of the simulation volume in an Al film energized to several energizations E_0; same simulations as those shown in Fig. 8. Density n has been normalized to the initial solid density, n_0. The molecular-dynamics trajectories (data taken every 0.2 ps) are compared to the phase diagram of Al (Fig. 3).

diagram of metals; consequently, melting precedes ablation for metals.

B. Transient void formation

Figure 4 compares void formation and decay (a) in a Lennard-Jones material and (b) in Cu. A computer animation can be found on the webpage in Ref. 33. The simulation data in Fig. 4(b) have been taken for Cu at an intensity corresponding to $E_0=0.8$ eV/atom ($\epsilon=0.23$). The pressure is on average tensile in the system, assuming values between −0.9 GPa at 4 ps and −0.3 GPa at 27 ps. In the middle of the slab a void nucleates at a time of roughly 4 ps. It grows and reaches its maximum thickness of around 26 Å at a time of 13 ps but then collapses again, until it vanishes at 29 ps.

For the purpose of comparison, the simulation data for the Lennard-Jones material [Fig. 4(a)] are presented in units of gigapascal; this is possible by choosing the Lennard-Jones parameters so as to describe the cohesive energy and the lattice parameter of Cu ($\epsilon=0.406$ eV, $\sigma=2.34$ Å). Note that in agreement with our finding of Fig. 2(a), a higher energization of $E_0=1.33$ eV/atom (corresponding to $\epsilon=0.37$) had to be chosen to realize the case of void formation. The stronger pressure fluctuations visible in the Lennard-Jones material are due to the increased energization of this material. Note the strong evaporation occurring in this material, which has already been visible in Fig. 1(a). At the earliest time, two voids are visible which coalesce later on.

Voids nucleate in the region where a large tensile pressure has formed. The actual location and time of formation of a void depend on statistics, i.e., on thermal fluctuations; this is identical to the usual case of phase nucleation, which is initiated by a critical nucleus which must be large enough to be able to grow. Void nucleation only occurs in the metastable region of the phase diagram.

The decay of a void could not be observed for simulations employing a narrower simulation volume, i.e., a simulation, in which the laterally periodic boundaries included too little volume. Thus, evidently, quantitative information on the fate of growing voids shows a strong size effect. The present simulations show, however, uniquely the qualitative feature of the possibility of void collapse. Furthermore, these simulations demonstrate the difficulty of an accurate quantitative prediction of the laser-ablation threshold by molecular-dynamics simulation without controlling lateral size effects. Anisimov and co-workers[3,11,28] denoted this material phase as a *foam*, since it is characterized by a mixture of liquid and gaseous materials.

C. Material expansion under irradiation

Figure 5 assembles data on the temporal variations of the thickness of a laser-irradiated film. A Cu film has been energized to four different energies E_0, $E_0=0.6$ and 0.7 eV/atom (below the ablation threshold), $E_0=0.8$ eV/atom (temporary void formation), and $E_0=0.9$ eV/atom (above the threshold). The first two cases (below threshold) lead to thermal expansion of the film; furthermore a series of oscillations is seen, which has been excited by the sudden irradiation. The period of these acoustic oscillations is quite constant for $E_0=0.6$ eV/atom and amounts to $2t_{\mathrm{sound}}=3.2$ ps, since the acoustic time is $t_{\mathrm{sound}}=1.6$ ps in molten Cu ($v_{\mathrm{sound}}=3.3$ km/s, $L=54$ Å) [Eq. (1)]. These oscillations become washed out and are more strongly damped in the molten material, $E_0=0.7$ eV/atom. The character of the oscillations changes as soon as internal voids are created. The last case (above threshold) demonstrates the free expansion of the torn material; a constant speed of the expansion front is observed after around 5 ps.

The most interesting case is that of the intermediate excitation, $E_0=0.8$ eV/atom; this case has been visualized atomistically in Fig. 4(b). The temporary formation of a void inside the irradiated film is reflected by the considerable bulging out of the surface. The thickness profile shows the expansion of the film to a maximum thickness of 100 Å. This value is by an amount of 23 Å larger than the final thickness of the molten film of 77 Å; the difference satisfactorily corresponds to the maximum void thickness, which was recorded as 26 Å (cf. Sec. III B). The time scale of this phenomenon reflects that of the lifetime of the void created [cf. Fig. 4(b)]. As noted above, the height of the surface elevation will depend to some degree on the lateral size of the simulation volume and is not meant to be predicted quantitatively by the present simulation. Also—for the idealized case of a fixed homogeneous energization of a foil with infinitively large surface—the height of the surface elevation will increase with the foil thickness.

After collapse of the void at $t=29$ ps, the system shows signs of oscillations, similar to the case of Fig. 2 discussed above. Note that during the lifetime of the void, the system does not oscillate; the appearance of the void, which in a larger simulation volume signals the entrance of the energized material into the two-phase region of the phase diagram, strongly dampens the initial oscillations.

We note that temporary void formation at laser fluences slightly below threshold has been observed earlier.[34] Reference 6 (Fig. 10) in addition also displays the accompanying surface excursions for the case of Si irradiation. The common feature that we wish to stress is not only the large amplitude of the swellings, which is connected to the size of the temporary voids, but in particular the extremely slow dynamics of the excursions. This dynamics is unrelated to the acoustic time t_{sound} [Eq. (1)], which otherwise governs the dynamics of the irradiated solid, but is determined by the nucleation, growth, and decay dynamics of these voids.

Recently, Temnov *et al.*[35,36] experimentally observed temporary surface excursions, which are similar to those described here. They applied high-precision ultrafast interferometric microscopy to directly monitor the dynamics of small transient surface deformations at laser irradiation fluences near the ablation threshold. For a Si target, at a laser fluence of 99% of the ablation threshold, the observed surface excursion lasted for around 150 ps and reached peak values of 10 nm; for GaAs, even 150 nm excursions were observed after a time of 5 ns after irradiation.

These are extremely long lasting surface excursions: their duration exceeds the acoustic time $t_{\mathrm{sound}}=d_{\mathrm{crat}}/c_s$ by a factor of 300, where $d_{\mathrm{crat}}\approx 40$ nm is the crater depth near the ablation threshold and $c_s\approx 2.5$ km/s is the sound velocity of liquid GaAs. In our simulation, for intermediate excitation,

E_0=0.8 eV/atom shown in Fig. 5, the surface excursion lasts $20t_{\text{sound}}$. We propose that the mechanism described here, viz., temporary void formation below the surface, is responsible for the extremely slow material response and hence for the experimental finding. The shorter space and time scales of the phenomenon observed in our simulations are thought to be due to the restricted size of our simulation volume. A further study of this dependence as well as of the strong material dependence observed in experiment (Si vs GaAs) is outside the scope of the present study.

D. Phase-space trajectories

The thermodynamics of an expanding liquid can be understood through the material pathway in the phase diagram, such as they have been introduced in Ref. 37 and used repeatedly since.[3,6,9,28] It is useful to plot the phase-space trajectories here because they help us to understand the superslow dynamics of the temporary void and also the absence of normal acoustic oscillations during the time the void exists. We shall see that this latter phenomenon is correlated with the phase-space trajectory forming a "loop" in phase space during which the system is highly damped and dissipates its kinetic energy.

Figure 6 plots phase-space trajectories for various initial energizations ϵ into a Lennard-Jones phase diagram. Here temperature and density have been averaged throughout the simulation volume. Note that these trajectories resemble the results of a previous study[9] for a *two-dimensional* Lennard-Jones semi-infinite system energized with exponentially decreasing intensity. Initially, the system is heated isochorically to a high temperature, from which it expands along an adiabat. For small energization, ϵ=0.20, the phase-space trajectory oscillates around the point of intersection of the adiabat with the two-phase coexistence boundary; the system is not yet molten. For ϵ=0.35, the phase-space trajectory passes through the triple-point region. As the atomistic visualization in Fig. 1(a) and the thresholds of Fig. 2 confirm, now the irradiated volume is about to melt. For even higher energization, ϵ=0.63, the system expands through the coexistence region ending in the vapor regime. Here, we are above the ablation threshold, and a binary mixture of vapor, large liquid droplets, and the spallation plates bounding the ablating film results [cf. Fig. 1(a)]. Figure 6 demonstrates that for the Lennard-Jones system, the threshold adiabat (introduced in Sec. III A) indeed passes slightly below the triple-point region of the phase diagram. Finally, the highest energization studied, ϵ=5, lets the system expand through the fluid region far above the critical point; it passes the binodal at a density of n=0.08, far below the critical density of n_c=0.31. This trajectory thus exemplifies the process of total disintegration of the film into a vapor cloud.

Since the ablation process is inherently inhomogeneous even for initial homogeneous energization, in the following we discuss phase-space trajectories obtained for the central third of the simulation volume. These data are presented in Fig. 7 for a Lennard-Jones crystal with the size of $36\times36\times30$ ML^3. In this case, the phase-space trajectories have been projected onto the (T-n), the (p-n), and the (p-T) planes. Four different energizations around the ablation threshold have been included, which span the range from crystal heating to vaporization (cf. the atomistic snapshots of Fig. 1 and the thresholds indicated in Fig. 2).

For the smallest energization, ϵ=0.19, the crystal is heated and acoustic oscillations are excited. In these, the temperature drops, when bonds are strained (decreasing density and tensile pressure) and kinetic energy is converted to potential energy. Consequently, the oscillations are visible in all three variable pairs—(T,n), (p,n), and (p,T)—plotted in Fig. 7.

For higher energizations, ϵ=0.31 and 0.33, the oscillations have changed to form a loop both in the (T-n) and in the (p-n) planes. The first part of the loop, leading to the minimum temperature and pressure, describes the response of the material during pressure relaxation: matter is cooled during the adiabatic expansion, and the pressure becomes strongly tensile. The temperature reached is around the triple-point value. However, in contrast to the oscillatory (almost reversible) behavior observed for smaller energization, the system continues expanding, while its temperature increases and the pressure is reduced to zero: This is due to the temporary formation of a void (two-phase mixture). Note that after the minimum density (maximum void volume) has been reached, the temperature stays almost constant, since the pressure is nearly zero, and the system does not do work by bond stretching.

Finally, for the largest energization of ϵ=0.38, the trajectory directly leads into the gas phase. Note that we plot only the quantities in the central part of the simulation; at the surfaces of the ablated film, liquid spallation plates remain (cf. Fig. 1). The initial expansion into the liquid-gas region is remarkably similar to the starting phase of the loop described above; here the same mechanism of cooling by expansion and subsequent void formation is operative. Then, however, the material tears, and its density is reduced to zero. Note that the maximum temperature reached by the gas is of similar magnitude as the final temperature for the smaller energizations; this temperature is below the critical temperature of the Lennard-Jones system, which is 1.35 in reduced Lennard-Jones units. The final drop of the temperature to zero in the gas phase is an artifact of our detector: when the gas density becomes too small, the detector volume contains too few atoms to analyze the variance of the velocity distribution, and hence the temperature is recorded as zero.

We note that a loop in the phase-space trajectory for subthreshold laser irradiation has been seen before in Si (Ref. 6, Fig. 11). The common feature we wish to stress is the extremely slow dynamics which governs the loop and which is unrelated to the acoustic time t_{sound} which otherwise controls the material response to the laser irradiation.

E. Comparison of molecular-dynamics results and thermodynamic analysis for Al

Figure 8 allows us to compare our molecular-dynamics simulation results with macroscopic thermodynamic considerations. To this end, the (p-n) trajectories of the central third of an Al simulation are plotted together with an ensemble of

isentropes obtained from an Al equation of state (EOS) based on Ref. 27. These isentropes are characterized in Fig. 8 by the temperature reached immediately after the isochoric energization.

Depending on the internal energy, which can be identified with the initial energizations E_0, the material behavior strongly varies. The pathways of the molecular-dynamics simulation are represented by trajectories where the separation between two points marking transient states is 0.2 ps.

For the lowest energy, $E_0=0.6$ eV/atom, the material expands along an isentrope, reaches its minimum value, relaxes to a pressure near zero while compressing again, and ends in acoustic oscillations at a smaller density than that of the initial state. For the energy $E_0=0.7$ eV/atom, the expansion initially resembles the case described above. However, after the pressure reached its minimum value, the material continues expanding while relaxing to zero pressure. Here, the similarity with the loops of Fig. 7 is obvious. The pressure remains slightly tensile, while the material compresses. This process takes place on a larger time scale than for $E_0=0.6$ eV/atom energization; it exemplifies the process of temporary void formation, which was highlighted for various materials in Figs. 1, 4, and 5. For the largest energization shown, $E_0=0.8$ eV/atom, the material continues expanding after reaching the maximum tensile stress (note that we record tensile stresses as negative quantities; however, in their discussion, we follow common usage and discuss the *absolute values* of the tensile pressure). After relaxation to almost vanishing pressure, the central part of the system expands until it finally is transformed to the gas phase.

As soon as a (temporary) void has formed ($E_0=0.7$ eV/atom), the material responds on a considerably enlarged time scale. From the thermodynamic point of view, this is due to the large decrease in the sound velocity, which occurs in two-phase materials. Note that the overall pressure during void collapse remains (slightly) negative; as a consequence, the void continues shrinking and the material does not tear. For the highest energization studied here ($E_0=0.8$ eV/atom), the final fragmentation and gasification of the central part of the film are reflected by the fact that the overall pressure is no longer tensile.

Remarkably, in all three cases the trajectories of the simulation initially follow quite well an adiabat. This good agreement between the simulation results and the thermodynamic analysis is satisfying. However, deviations occur as soon as the two-phase region is entered and the pressure has become tensile. The maximum tensile stress in all cases is $|p| \cong 6$ GPa. After reaching this value, strong deviations occur.

Figure 9 displays our simulation results in the (T,n) plane and sets them in relation to the phase diagram of Al (cf. Fig. 3). A comparison with the Lennard-Jones data of Fig. 7 shows a qualitatively similar dependence, in particular with respect to the loops which form at near-threshold energization. However, for Al, all near-threshold trajectories cross the binodal from the liquid region of the phase diagram. This is in strong contrast to the behavior of the Lennard-Jones system, where the threshold adiabat crosses the binodal without touching the liquid phase.

Quantitatively, in our Al thin film the threshold adiabat crosses the binodal at around $1.9T_{\mathrm{tr}} \cong 1750$ K, while for the Lennard-Jones system, the crossing takes place at $0.47T_c \cong 1.0T_{\mathrm{tr}}$ at the triple point. It is appropriate to compare with the results of Petrov *et al.*,[32] who investigated the threshold adiabat for a thick Al targets with inhomogeneous, i.e., exponentially decreasing, laser heating. They found that the threshold adiabat crosses the binodal at $2.2T_{\mathrm{tr}} \cong 2000$ K, while for our ultrathin target the crossing takes place at around 1750 K. It is known from other studies[29] that in thick systems the location of the threshold adiabat in the phase diagram is shifted to slightly higher temperatures. Our present simulation results show that also for thin freestanding films, Al is in the liquid phase when the threshold adiabat crosses the binodal line.

We note that a previous study[9] demonstrated that a two-dimensional Lennard-Jones film ablates from the solid state. Also, the ablation of organic solids starts at threshold laser fluences from the solid state.[34] The fact that already at threshold metals ablate from the liquid state has been observed previously in several investigations.[4,38] In the present work, we relate this different behavior to the phase diagrams of these materials (cf. Figs. 7 and 9). The phase diagrams of course originate from the interatomic potentials in the materials and hence reflect the different bonding types. As is well known,[39] it is exactly the many-body nature of metallic bonding which is responsible for decreasing the melting point with respect to a pair-bonded (i.e., Lennard-Jones-type) material (cf. Fig. 3). Certainly, a full explanation of the relations between the phase diagram (or equation of state) of a material and the properties of its threshold adiabat will require further investigations. We also note that in Si, a prototype of a covalently bonded material, the threshold adiabat also passes through the liquid state.[6]

From the thermodynamic point of view, isentropic expansion may proceed up to a certain maximum tensile stress $|p_{\mathrm{spinodal}}|$, which is given by the minimum of the expansion isentrope, and occurs at the point, where the adiabat reaches the spinodal line of the phase diagram. It is the maximum tensile pressure which a rapidly strained material may sustain before it becomes (thermodynamically) unstable. For slow expansion, this value is unlikely to be reached since the gas phase will start nucleating already before the spinodal line is reached. For the fast expansion processes investigated in the present simulations, however, the phase-space trajectory may come close to the spinodal line, which forms the ultimate limitation of the metastable region.

Evidently, the thermodynamic analysis—i.e., the expansion along an isentrope—is valid only until the expansion approaches the spinodal point; the ensuing material instability has to be modeled using an atomistic approach. The small deviations between molecular dynamics and the thermodynamic approach occurring (for tensile pressures) before the spinodal is reached are assumed to be due to the fact that both the interatomic potentials[18] used in the simulation, and the equation of state,[27] from which the isentropes have been constructed, do possibly not correctly describe the hot and strongly strained state of Al encountered here.

It is certainly possible to apply the hydrodynamic approach (using an EOS and adding phenomenological kinetics) to describing the spallation. Spallation is assumed to start as soon as the tensile pressure $|p|$ exceeds a material

dependent limit, the spall strength. Three simple criteria for the onset of spallation may be formulated: (i) matter decomposes near the binodal, (ii) matter decomposes near the spinodal, or (iii) matter decomposes when its tensile pressure $|p|$ is equal to the strength limit of material. Therefore molecular dynamics significantly supplements the hydrodynamic approach in the sense that it follows real kinetics and can judge between these three models (binodal, spinodal, and the strength limit).

In fact, our calculations show that near the ablation threshold the stretched material nucleates metastably already rather far from the spinodal. However, these detailed features of the nucleation process are outside of the scope of the present work, and further investigations are needed to quantify these results and to compare them with genuinely hydrodynamic approaches to spallation, such as that of Ref. 40.

IV. CONCLUSIONS

The materials physics operative close to the ablation threshold exhibits a wide variety of phenomena, ranging from melting over the temporary formation of voids or gas bubbles to the tearing of the material. The materials processes show the same general characteristics for such widely different materials as Lennard-Jones materials and metals. However, while metals generally ablate in the liquid state, Lennard-Jones materials spall in the solid state for energizations close to the ablation threshold. This difference is due to a generic difference in the phase diagram of these materials; the liquid phase covers a wider region in the phase diagram of metals than of Lennard-Jones materials. Immediately below the ablation threshold, voids or gas bubbles nucleate in the material. The resulting two-phase (foamy) structure is initially under strong tensile stress. The ablation threshold is characterized by a tensile stress which exceeds the yield strength of this foamy structure, such that the material tears. The nucleation of voids leads to a characteristic temporary expansion of the irradiated material, which is clearly distinguishable from the acoustic oscillations occurring at lower laser intensities and the ablation process occurring at higher intensity. It has been observed experimentally. Comparison of the molecular-dynamics results with the macroscopic thermodynamics of the material shows good agreement: the expansion of the energized material proceeds along an isentrope until deep into the two-phase coexistence zone. However, as soon as too large tensile pressures are created and a foamy structure forms, the phase-space trajectory leaves the isentrope, while the material relaxes toward zero pressure. The thermodynamic analysis loses its validity, as soon as the phase-space trajectory reaches the vicinity of the spinodal line, and the metastable material decomposes into a two-phase mixture.

ACKNOWLEDGMENTS

The authors acknowledge stimulating discussions with S. I. Anisimov, D. von der Linde, K. Sokolowski-Tinten, V. V. Temnov, and V. V. Zhakhovskii, as well as financial assistance by the Deutsche Forschungsgemeinschaft via the Graduiertenkolleg 792, which enabled the visits of B.R. and N.A.I. during the time this work was prepared. B.R. and H.M.U. acknowledge support by the BMBF (Grant No. FSP 301 FLASH) and N.A.I. by the RFBR (Grant No. 07-02-00764).

*urbassek@rhrk.uni-kl.de; http://www.physik.uni-kl.de/urbassek/

[1] S. I. Anisimov, N. A. Inogamov, A. M. Oparin, B. Rethfeld, T. Yabe, M. Ogawa, and V. Fortov, Appl. Phys. A: Mater. Sci. Process. **69**, 617 (1999).
[2] N. A. Inogamov, Y. V. Petrov, S. I. Anisimov, A. M. Oparin, N. V. Shaposhnikov, D. von der Linde, and J. Meyer-ter-Vehn, JETP Lett. **69**, 310 (1999).
[3] V. V. Zhakhovskii, K. Nishihara, S. I. Anisimov, and N. A. Inogamov, JETP Lett. **71**, 167 (2000).
[4] C. Schäfer, H. M. Urbassek, and L. V. Zhigilei, Phys. Rev. B **66**, 115404 (2002).
[5] D. S. Ivanov and L. V. Zhigilei, Phys. Rev. B **68**, 064114 (2003).
[6] P. Lorazo, L. J. Lewis, and M. Meunier, Phys. Rev. B **73**, 134108 (2006).
[7] S. I. Anisimov, V. V. Zhakhovski, N. A. Inogamov, K. Nishihara, Y. V. Petrov, and V. A. Khokhlov, Sov. Phys. JETP **103**, 183 (2006).
[8] D. S. Ivanov and L. V. Zhigilei, Phys. Rev. Lett. **91**, 105701 (2003).
[9] D. Perez and L. J. Lewis, Phys. Rev. B **67**, 184102 (2003).
[10] A. K. Upadhyay and H. M. Urbassek, Phys. Rev. B **73**, 035421 (2006).
[11] M. B. Agranat, S. I. Anisimov, S. I. Ashitkov, V. V. Zhakhovskii, N. A. Inogamov, K. Nishihara, Y. V. Petrov, V. E. Fortov, and V. A. Khokhlov, Appl. Surf. Sci. **253**, 6276 (2007).
[12] L. V. Zhigilei, E. Leveugle, B. J. Garrison, Y. G. Yingling, and M. I. Zeifman, Chem. Rev. (Washington, D.C.) **103**, 321 (2003).
[13] S. I. Anisimov, B. L. Kapeliovich, and T. L. Perel'man, Sov. Phys. JETP **39**, 375 (1974).
[14] K. Furusawa, K. Takahashi, H. Kumagai, K. Midorikawa, and M. Ohara, Appl. Phys. A: Mater. Sci. Process. **69**, S359 (1999).
[15] A. K. Upadhyay and H. M. Urbassek, J. Phys. D **40**, 3518 (2007).
[16] A. K. Upadhyay and H. M. Urbassek, J. Phys.: Conf. Ser. **59**, 68 (2007).
[17] H. Gades and H. M. Urbassek, Nucl. Instrum. Methods Phys. Res. B **69**, 232 (1992).
[18] F. Ercolessi and J. B. Adams, Europhys. Lett. **26**, 583 (1994).
[19] X. W. Zhou *et al.*, Acta Mater. **49**, 4005 (2001).
[20] A. K. Upadhyay and H. M. Urbassek, J. Phys. D **38**, 2933 (2005).
[21] T. J. Colla and H. M. Urbassek, Radiat. Eff. Defects Solids **142**, 439 (1997).
[22] F. H. Ree, J. Chem. Phys. **73**, 5401 (1980).
[23] B. Smit, J. Chem. Phys. **96**, 8639 (1992).
[24] Y. Choi, T. Ree, and F. H. Ree, J. Chem. Phys. **99**, 9917 (1993).

[25] D. A. Kofke, J. Chem. Phys. **98**, 4149 (1993).
[26] R. Agrawal and D. A. Kofke, Mol. Phys. **85**, 43 (1995).
[27] A. V. Bushman, G. I. Kanel', A. L. Ni, and V. E. Fortov, *Intense Dynamic Loading of Condensed Matter* (Taylor & Francis, Washington, DC, 1993).
[28] S. I. Anisimov, V. V. Zhakhovski, N. A. Inogamov, K. Nishihara, A. M. Oparin, and Y. V. Petrov, JETP Lett. **77**, 606 (2003).
[29] S. I. Anisimov, V. V. Zhakhovskii, N. A. Inogamov, K. Nishihara, and Y. V. Petrov, Appl. Surf. Sci. **253**, 6390 (2007).
[30] B. V. Deryagin, Zh. Eksp. Teor. Fiz. **65**, 2261 (1973) [Sov. Phys. JETP **38**, 1129 (1974)].
[31] V. P. Skripov and M. Z. Faizullin, *Crystal-Liquid-Gas Phase Transitions and Thermodynamic Similarity* (Wiley, Berlin, 2006).
[32] Y. V. Petrov, S. I. Anisimov, N. A. Inogamov, V. A. Khokhlov, V. V. Zhakhovski, K. Nishihara, A. K. Upadhyay, B. Rethfeld, and H. M. Urbassek, in Proceedings of the XXIII International Conference on Physics of the Extreme States of Matter (Russian Academy of Sciences, Chernogolovka, 2008), p. 175 (in Russian).
[33] http://www.physik.uni-kl.de/urbassek
[34] L. V. Zhigilei and B. J. Garrison, J. Appl. Phys. **88**, 1281 (2000).
[35] V. V. Temnov, Ph.D. thesis, University of Duisburg-Essen, 2004.
[36] V. V. Temnov, K. Sokolowski-Tinten, P. Zhou, and D. von der Linde, J. Opt. Soc. Am. B **23**, 1954 (2006).
[37] K. Sokolowski-Tinten, J. Bialkowski, A. Cavalleri, D. von der Linde, A. Oparin, J. Meyer-ter-Vehn, and S. I. Anisimov, Phys. Rev. Lett. **81**, 224 (1998).
[38] C. Cheng and X. Xu, Phys. Rev. B **72**, 165415 (2005).
[39] M. I. Baskes, Phys. Rev. Lett. **83**, 2592 (1999).
[40] F. Vidal, T. W. Johnston, J. C. Kieffer, and F. Martin, Phys. Rev. B **70**, 184125 (2004).
[41] H. M. Urbassek, in *Handbook of Surface Science, Dynamics*, edited by E. Hasselbrink and B. Lundvist (Elsevier, Amsterdam, 2008),Vol. 3.